Eurasian Chem.-Technol. J. 27 (2025) 289–303
The journal of the Institute of Combustion Problems https://ect-journal.kz

https://doi.org/10.18321/ectj1676

Influence of Modified Polyvinyl Caprolactam on Methane Hydrate Formation: Structural and Morphological Insights

Marwah N. Mohammed

Chemical Engineering Department, College of Engineering, Tikrit University, Tikrit, Iraq

Article info

Received:
18 July 2025

Received in revised form:
16 September 2025

Accepted:
26 October 2025

Keywords:
Methane hydrate inhibition
Polyvinyl caprolactam (PVCap)
Hydrate formation control
Kinetic inhibitors
Pipeline hydrate management

Abstract

Controlled injection of kinetic hydrate inhibitors (KHIs) is one of the most effective flow-assurance strategies for delaying hydrate nucleation and crystal growth in multiphase natural gas pipelines. To enhance the structure of the kinetic inhibitor polyvinyl caprolactam (PVCap), oxyethyl and ester functional groups were introduced, resulting in the development of a new inhibitor, PVCap-XA1. PVCap-XA1 has been applied to achieve enhanced inhibition performance against methane hydrate formation. The structural and morphological changes in methane hydrates formed in the presence of PVCap-XA1 were investigated using advanced characterization techniques, including PXRD, low-temperature Raman spectroscopy, and cryo-SEM. Under identical experimental conditions, PVCap-XA1 demonstrates higher kinetic inhibition efficiency compared with PVCap. Microscopic analysis indicates that the clathrate structure of methane hydrate remains unchanged; however, PVCap-XA1 induces lattice-plane distortions that result in smaller crystallites. In the presence of PVCap-XA1, the induction time for hydrate formation was extended to approximately 240 min, and the maximum subcooling increased to 10.8 °C, compared with 8.1 °C for PVCap. In addition, PVCap-XA1 alters the cage occupancy ratio (IL/IS), making it more difficult for methane molecules to occupy hydrate cages. PVCap-XA1 also modifies the microscopic morphology of methane hydrate, shifting it from a porous to a dense, compact structure. This densification blocks gas flow through the hydrate layer, further enhancing inhibition efficiency. Overall, the results demonstrate that PVCap-XA1 is a promising kinetic inhibitor capable of addressing industrial challenges associated with methane hydrate formation in pipelines.

1. Introduction

Natural gas hydrates are crystalline clathrates – frozen solids that form under high-pressure, low-temperature conditions when water encapsulates small guest gas molecules (e.g., CH_4, C_2H_6, CO_2, H_2S). The water phase organizes into a hydrogen-bonded network of polyhedral cavities that encapsulate the gas guests [1, 2]. Based on lattice topology, hydrates can be structure I (sI), structure II (sII), or structure H (sH) [3].

These well-studied materials have significant potential as future energy sources and gas-storage carriers; however, they also present operational challenges for oil and gas production systems. The formation of solid hydrates within pipelines and equipment during drilling, transportation, and processing can cause severe blockages, equipment failures, and costly downtime. Such incidents are not only dangerous but may also lead to substantial economic losses and environmental risks [4, 5]. These issues are addressed through various preventive measures, such as pressure control, pipeline heating, and chemical inhibitor injection. Among these approaches, chemical inhibitors are the most effective and commonly used solution. These com-

*Corresponding author.
E-mail address: marwa.n.mohammed@tu.edu.iq

pounds act at the early stages of hydrate formation by preventing crystal nucleation and limiting subsequent growth, thereby delaying or even preventing hydrate buildup [6]. Hydrate inhibitors are generally classified into two major groups: thermodynamic inhibitors (THIs) and low-dose kinetic hydrate inhibitors (KHIs). THIs, such as methanol, ethylene glycol, and aqueous electrolyte solutions, suppress hydrate formation by shifting the thermodynamic equilibrium toward lower temperatures and/or higher pressures. These inhibitors must be added in substantial quantities, typically 10–50% of the water phase by mass, which makes the process expensive. Moreover, methanol, the most widely used THI, is toxic and poses environmental concerns [7, 8].

Low-dose hydrate inhibitors, including KHIs and anti-agglomerants, offer a more economical and environmentally favorable alternative. Anti-agglomerants prevent the agglomeration of hydrate particles into larger masses, while KHIs suppress hydrate formation by inhibiting nucleation and growth. Of these, KHIs are favored in natural gas pipelines due to their effectiveness at much lower concentrations, typically in the range of 0.01–5% by mass [9].

Water-soluble polymers, especially polyvinylpyrrolidone (PVP) and polyvinylcaprolactam (PVCap), are widely used as kinetic hydrate inhibitors [10]. PVP is one of the first-generation KHIs and prevents crystal growth by adsorbing onto advancing hydrate faces via five-membered lactam-ring-mediated interactions [11]. However, its inhibitory effectiveness is highly temperature-dependent and diminishes below 12 °C [12]. A second-generation inhibitor, PVCap, is a polymer based on a seven-membered lactam ring and exhibits better inhibition performance than PVP [13]. It has been reported that 0.5% PVCap by mass at a supercooling degree of 8–9 °C can delay hydrate nucleation for up to 24 h, although its effectiveness decreases over time [14].

Despite these advances, most existing kinetic inhibitors, such as PVCap, suffer from limitations under variable industrial environmental and operating conditions [15]. Consequently, recent research has focused on modifying these polymers to enhance their inhibitory efficiency. One approach involves introducing functional groups to improve inhibitor properties [16, 17]. For example, hydrophilic groups such as carboxyl groups have been added to PVCap, resulting in derivatives with enhanced methane hydrate inhibition efficiency [18]. Similarly, hydrophobic modifications of PVP-based inhibitors, such as the incorporation of alkyl groups, have also improved overall performance [19].

Additionally, copolymerization methods have proven effective for enhancing inhibitor performance [20]. For example, copolymerizing PVCap with monomers such as ethylene glycol methyl ether, methacrylate, or vinylimidazole has yielded new inhibitors with improved ability to delay hydrate nucleation and growth [21]. However, most investigations have focused on introducing a single functional group or implementing only limited structural modifications.

Although these studies demonstrate that PVCap modification can enhance performance, a comprehensive understanding of the synergistic effects resulting from multiple functional-group alterations remains limited [22]. In particular, the simultaneous introduction of both hydrophilic and hydrophobic groups to PVCap has not been widely studied. To date, fewer than five studies have reported PVCap derivatives containing dual terminal functionalities, highlighting a significant knowledge gap regarding their combined influence on hydrate inhibition. More importantly, only a few of these reports have related such molecular modifications to changes in hydrate crystal structure and morphology, which are critical for optimizing inhibitor performance.

The newly synthesized inhibitor, PVCap-XA1, carries oxyethylene (hydrophilic) and ester (hydrophobic) functional groups at the polymer chain termini. These groups were introduced to achieve an optimal balance between polarity and molecular flexibility. The oxyethylene moieties enhance hydrogen bonding with interfacial water molecules, thereby strengthening polymer–hydrate surface interactions, whereas the ester groups create localized hydrophobic domains that disrupt the structured hydrogen-bond network of water and reduce its ability to form stable hydrate cages. In this dual-functional configuration, the inhibitor is expected to provide superior kinetic performance by simultaneously promoting surface adsorption and locally perturbing the water structure.

This study addresses these gaps by synthesizing the modified kinetic inhibitor PVCap-XA1, which bears both oxyethylene (hydrophilic) and ester (hydrophobic) groups at the polymer chain termini. Fourier-transform infrared (FTIR) spectroscopy and ^{1}H NMR spectroscopy confirmed the successful incorporation of the target functional groups in PVCap-XA1. Performance evaluation was conducted under controlled laboratory conditions using constant-volume/constant-temperature and uniform-cooling procedures to assess inhibition of methane hydrate formation. Additional characterization methods, including powder X-ray diffraction (PXRD), low-temperature

Raman spectroscopy, and cryo-SEM, were employed to determine lattice order, guest–host interactions, and microstructural morphology, respectively.

The study confirms that PVCap-XA1 is a more effective inhibitor than PVCap and induces notable microstructural changes, including reduced crystallite size and increased compaction. Collectively, these results provide valuable guidance for designing and applying next-generation hydrate inhibitors in flow-assurance processes, supporting the development of more environmentally friendly applications.

2. Experimental materials and methods

2.1. Material

All chemicals were of analytical grade and used as received to ensure consistency across all experiments. Potassium ethyl xanthate (98%), methyl 2-bromopropionate (87%), ethanol (≥99.7%), methylene chloride (≥99.8%), sterilized water (≥99.99%), anhydrous magnesium sulfate (99.99%), and 2,2'-azobisisobutyronitrile (AIBN, ≥98.0%) were obtained from Sigma-Aldrich (Malaysia). N-vinylcaprolactam (NVCap, ≥98.0%) was purchased from Shanghai Tixiai Chemical Industry Co., Ltd.; 1,4-dioxane (≥99.5%) from Shanghai Aladdin Biochemical Technology Co., Ltd.; n-hexane (97%) from Shanghai McLean Company; and methane gas (≥99.0%) from Sigma-Aldrich. Distilled water was prepared in-house at Universiti Malaysia Pahang and used without further purification.

2.2. Inhibitor synthesis

The chain transfer agent XA1 was purified by rotary evaporation under reduced pressure at 85 °C to remove the bulk solvent. The cooled residue was diluted with 25 mL of deionized water, transferred to a separatory funnel, and extracted three times with 50 mL of methylene chloride (CH_2Cl_2). The combined extracts were washed with water, dried over anhydrous $MgSO_4$, filtered, and concentrated in vacuo to yield a yellow oil (Fig. 1).

All syntheses were performed in triplicate to assess reproducibility. The average isolated yields were 69.7 ± 1.2% for PVCap-XA1 and 63.2 ± 1.5% for PVCap, with consistent recoveries across runs, confirming reproducibility. These results indicate that XA1 improved molecular control while maintaining consistent reaction efficiency.

Modified inhibitors were synthesized under air-free conditions. To prepare PVCap-XA1, NVCap (13.92 g, 0.1 mol), AIBN (16.67 mg, 0.1 mmol), and XA1 (50 mg, 0.24 mmol) were dissolved in 5 mL of 1,4-dioxane in a 50-mL round-bottom flask. The flask was tightly sealed and purged with nitrogen three times to ensure complete isolation from atmospheric air.

The reaction mixture was heated at 60 °C in an oil bath under a continuous nitrogen flow to maintain an inert atmosphere. The reaction proceeded for approximately 6 h, after which the flask was cooled to 2 °C for 20 min. The product was purified by precipitation in hexane, yielding PVCap-XA1 in 69.7%

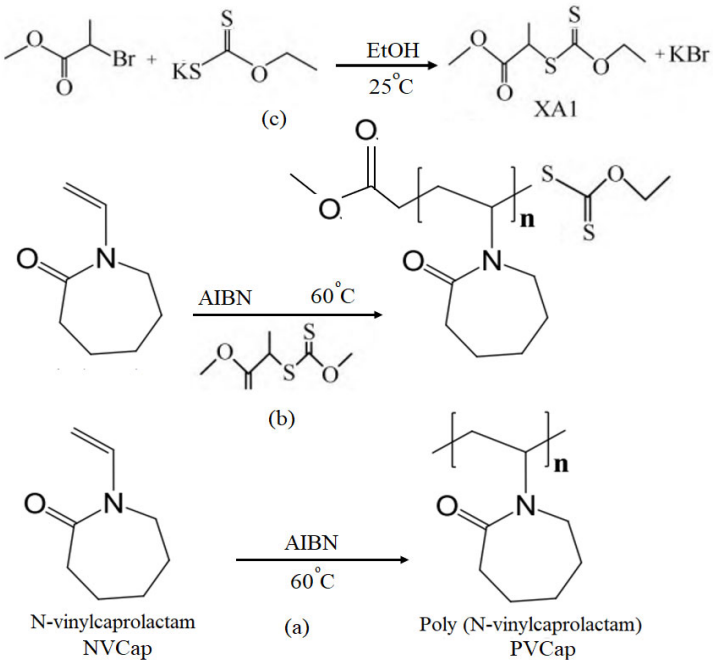

Fig. 1. Route Development and Synthesis of XA1, PVCap, and PVCap-XA1.

yield (Fig. 1b). Unmodified PVCap was synthesized following the same procedure, without the addition of XA1, and obtained in 63.2% yield (Fig. 1c). These results demonstrate that the synthetic protocol is efficient and that the use of XA1 improves molecular control while maintaining consistent reaction efficiency.

2.3. Inhibition performance test

2.3.1. Experimental device

Briefly, the equipment includes a stainless-steel reactor with a high-pressure trap, a water bath maintained at a constant temperature, a pre-cooled gas buffer tank, a magnetically coupled stirrer, and a data-acquisition system linked to a computer for logging every 10 seconds. Induction times were measured under isothermal, constant-volume conditions in a 100 mL reactor (MAWP 20 MPa) built according to Tang et al. [22]. To determine the maximum subcooling under constant-volume, uniform-cooling conditions (Fig. 2), a 40 mL sapphire reactor rated at 12 MPa was used. Agitation was controlled from 0 to 1200 rpm. Pressure was measured using a CYB-20S transducer (0–20 MPa, ±0.025 MPa), and temperature was measured with a PT100 RTD (−40 to 100 °C, ±0.1 °C). The reactor assembly was housed inside a WGD/J-108 low-temperature test chamber.

2.3.2. Experimental process

The constant-temperature, constant-volume method quantifies the induction time of inhibitor solutions, a critical parameter for understanding the kinetics of hydrate formation in the presence of inhibitors. This experimental setup fills the high-pressure stainless-steel reaction vessel with 30 mL of the inhibitor solution. This vessel is subsequently placed in a constant-temperature bath maintained at 4 °C. Once the solution reaches thermal equilibrium at this temperature, the system should be evacuated to a vacuum, and methane gas is then introduced until the internal pressure reaches 8 MPa. After temperature and pressure stabilize, valve A is closed, and the magnetic stirrer is turned on at 1000 r/min. The induction time (t_i) is defined as the period between the start of stirring and the subsequent development of a pressure drop, signaling the onset of hydrate nucleation, i.e., the formation of the first hydrate crystal. This timeframe is crucial for assessing how effectively an inhibitor delays hydrate formation under controlled conditions.

In this method, constant-volume, constant-rate cooling is applied to measure the maximum subcooling of inhibitor solutions, reflecting the degree to which the solutions can be subcooled before hydrate formation below the equilibrium hydrate formation temperature. This technique adds 10 mL of the inhibitor solution to a sapphire reactor. First, the reactor is evacuated to a vacuum; then, methane gas is fed into the reactor up to a pressure of 9 MPa. After stabilizing the pressure, the gas inlet valve is closed, and the magnetic stirrer is turned on at 900 rpm. Afterward, the system undergoes programmed cooling in an air bath at a constant rate of 1 °C/h. The temperature gradually decreases from +20 °C to -10 °C to induce hydrate formation.

During cooling, the formation of methane hydrates is indicated by two key indicators: a sudden pressure drop and a slight temperature rise. The pressure drop is a result of hydrate formation, while the temperature rise is attributed to the exothermic nature of hydrate crystallization. The temperature at which hydrate formation starts is recorded as T_0, assumed to be the onset temperature of hydrate formation. The maximum degree of subcooling was then calculated as the difference between the hydrate equilibrium temperature at the observed pressure and the recorded temperature (T_0). This maximum subcooling value is a crucial metric for evaluating the solution's inhibitory efficiency in delaying hydrate formation during cooling.

These two methods, the constant-temperature, volume method and the continuous-rate cooling method, quantify induction time and subcooling capability and provide essential data on the performance of hydrate inhibitors. Such data are critical for evaluating inhibitor effectiveness and guiding the development of more efficient strategies for hydrate control in natural gas and petroleum systems.

2.3.3. Preparation of hydrate samples

Thirty milliliters of inhibitive solution were loaded into a high-pressure stainless-steel reactor, which was then equilibrated at 4 °C in a constant-temperature water bath. After thermal stabilization, the reactor was evacuated and charged with methane to 10 MPa. The gas line was closed, and the mixture was agitated at 1000 rpm. Hydrate formation was indicated by an abrupt pressure drop accompanied by a gradual temperature increase. The reactor pressure subsequently stabilized, and the system remained undisturbed for approximately one week. After one week, the reactor was removed from the water bath, and its outer surface was quickly dried

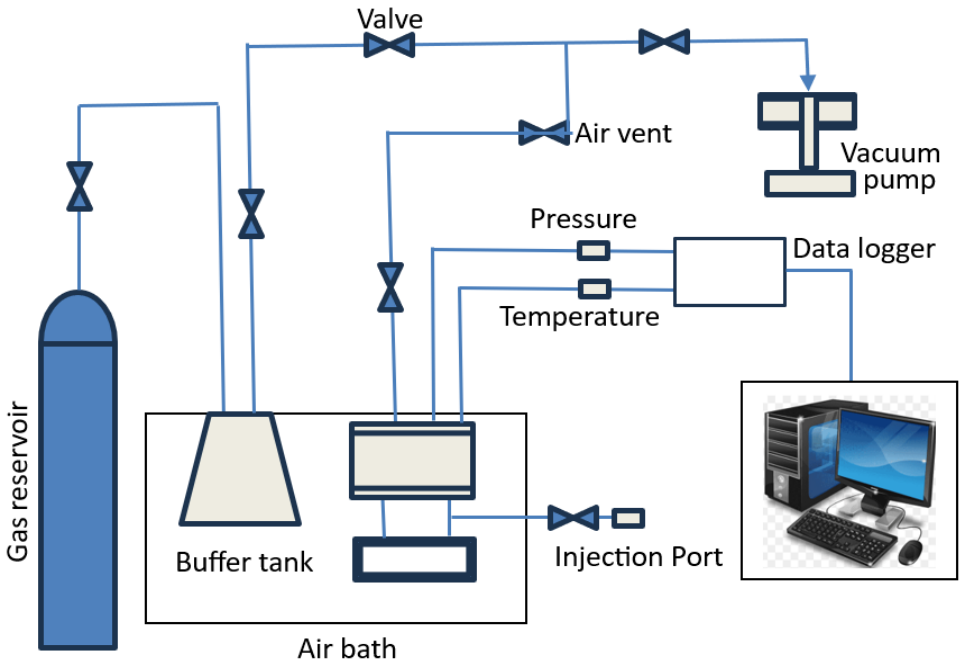

Fig. 2. Schematic representation of the laboratory setup employed in kinetic hydrate inhibition measurements.

to remove residual moisture. The hydrate sample was immediately immersed in an insulated container filled with liquid nitrogen for rapid freezing (2 min). The sample was then transferred under liquid nitrogen protection into a pre-cooled cryogenic tube and stored in a liquid nitrogen tank.

For powder X-ray diffraction (XRD) analysis, the cryogenic tube was removed, and the hydrate sample was placed in a pre-cooled mortar filled with liquid nitrogen. The sample was briefly frozen and then ground into a fine powder under continuous nitrogen protection. The powder was promptly transferred to the groove of the XRD sample stage for analysis.

For Raman spectroscopy, the hydrate sample was similarly transferred from the cryogenic tube into a pre-cooled mortar, where it was gently ground into particles approximately 1 mm in diameter. The particles were then transferred to a quartz crucible, sealed, and analyzed under a liquid nitrogen purge.

For low-temperature scanning electron microscopy (SEM), the hydrate was ground in a pre-cooled mortar to particles approximately 1–2 mm in size. The particles were placed into a pre-folded tinfoil groove under nitrogen protection, tightly packed, and pre-processed in the refrigerated conveying system prior to imaging.

2.4. Structural characterization

PVCap-XA1, PVCap, and the monomer NVCap were characterized using Fourier Transform Infrared (FTIR) and Nuclear Magnetic Resonance (NMR) spectroscopy. FTIR spectra were recorded on a Bruker TENSOR27 spectrometer, with samples prepared as potassium bromide (KBr) pellets to ensure consistency and improve spectral quality.

^{1}H NMR spectra of PVCap-XA1 and PVCap were recorded using a Bruker AVANCE III spectrometer. Samples were dissolved in deuterated chloroform ($CDCl_3$) as the solvent. The spectra provided detailed information on the hydrogen environments within the polymers, confirming their molecular structures

The crystallography of methane hydrate was analyzed using a powder X-ray diffractometer (X'Pert Pro MPD, PANalytical) at 50 °C and atmospheric pressure. Diffraction patterns were recorded over a 2θ range of 5°–80°, allowing determination of the crystal structure and lattice parameters of the hydrate phase.

The occupancy of the hydrate cages was assessed using low-temperature Raman spectroscopy. Spectra were recorded at –196 °C and atmospheric pressure using an Ar^+ laser (532 nm) at 50 mW. The Raman spectra provided detailed information on the spatial arrangement and occupancy of the hydrate cages.

Cryo-scanning electron microscopy (cryo-SEM, Hitachi S-4800) was used to investigate the morphology of gas hydrate crystals. Imaging was performed at –140 °C under vacuum to minimize thermal or pressure-induced artifacts, providing high-resolution images of hydrate surfaces and enabling analysis of crystal growth patterns and physical characteristics.

3. Results and Discussion

3.1. Structural characterization of XA1, PVCap-XA1 and PVCap

3.1.1. FTIR characterization results

Figure 3 shows the FTIR spectra of NVCap, PVCap, and PVCap-XA1. The 1080 cm^{-1} and 1195 cm^{-1} peaks correspond to C–N bending vibrations within the caprolactam ring, while the 1626 cm^{-1} peak is associated with lactam C=O stretching [23, 24]. In NVCap, the 1665 cm^{-1} band corresponds to C=C stretching in the monomer, and the 3109 cm^{-1} peak is assigned to C–H stretching.

The spectra of PVCap and PVCap-XA1 confirm that the core PVCap structure is preserved, as the C=O and C–N bands remain. The disappearance of the 1665 cm^{-1} and 3109 cm^{-1} peaks in PVCap-XA1 indicates that the monomer reacted during polymerization.

A prominent band at 1046 cm^{-1} in PVCap-XA1 is attributed to C=S stretching introduced via the XA1 chain-transfer agent. The broad O–H stretching band around 3447 cm^{-1} reflects increased hydrophilicity due to oxyethylene incorporation. These features, absent in unmodified PVCap, confirm successful terminal modification while retaining the core lactam structure.

3.1.2. ^{1}H NMR characterization results

Figure 4 shows the ^{1}H NMR spectra of N-vinylcaprolactam (NVCap), poly(N-vinylcaprolactam) (PVCap), and the modified PVCap-XA1. In the spectrum of the chain transfer agent XA1, characteristic chemical shifts are observed at δ = 3.75 ppm (3H, s, –OCH_3), 4.38 ppm (1H, q, –$CHCH_3S$–), and 4.62 ppm (2H, q, –OCH_2CH_3).

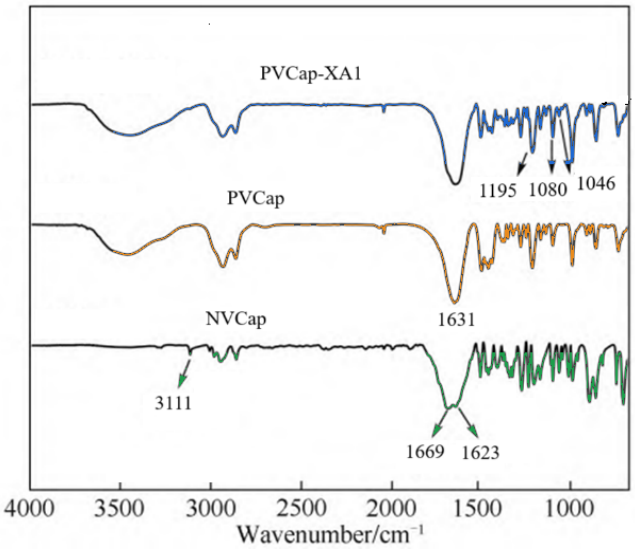

Fig. 3. FTIR spectra of N-vinylcaprolactam (NVCap), poly(N-vinylcaprolactam) (PVCap), and PVCap-XA1.

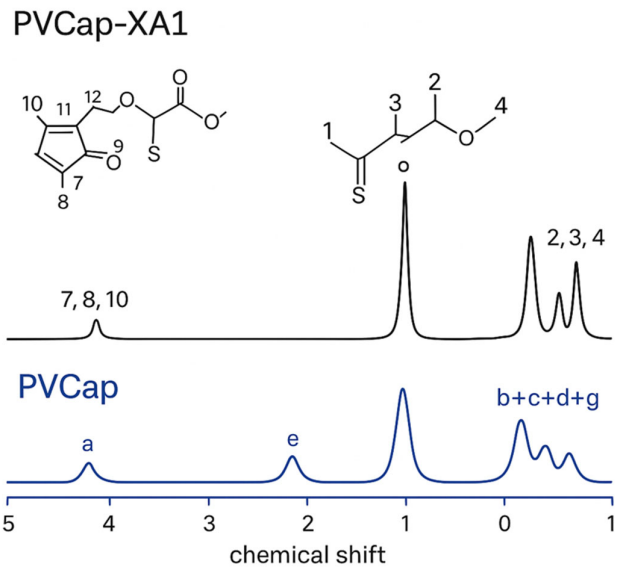

Fig. 4. ^{1}H NMR spectra of N-vinylcaprolactam (NVCap), poly(N-vinylcaprolactam) (PVCap), and PVCap-XA1.

In PVCap-XA1:

- δ = 4.25–4.65 ppm represents the peaks (“7, 8, 10”) of —CH— protons in —NCH—, —OCH_2—, and —$CHCH_3$—.
- δ = 3.65 ppm corresponds to —OCH_3 protons from ester linkages (“12”).
- δ = 2.88–3.46 ppm corresponds to —NCH_2— protons (“1”).
- δ = 2.23–2.70 ppm corresponds to —$COCH_2$— protons (“5”).
- δ = 1.50–2.00 ppm corresponds to caprolactam ring —CH_2— protons (“2, 3, 4”).
- δ = 1.00–1.50 ppm corresponds to —CH_3 in —OCH_2CH_3, —$CHCH_3$—, and main-chain—CH_2— protons (“6, 9, 11”).

In PVCap, the chemical shifts of the backbone protons are similar, indicating that the main PVCap structure is preserved.

Comparison of PVCap and PVCap-XA1 confirms that the polymer backbone remains intact. New peaks at δ = 3.65 ppm and δ = 4.25–4.65 ppm in PVCap-XA1 correspond to ester and oxyethylene linkages introduced via the XA1 chain-transfer agent; these peaks are absent in unmodified PVCap, confirming the introduction of both hydrophilic and hydrophobic substituents.

The chemical shifts of lactam ring protons (δ = 1.0–2.8 ppm) remain unchanged in both polymers.

Additionally, the FTIR spectrum of PVCap-XA1 shows a band at 1046 cm^{-1} assigned to C=S stretching, further confirming successful synthesis.

Together, the FTIR and ^1H NMR data confirm the dual-functional modification of PVCap while preserving the integrity of its backbone.

3.2. Inhibitory effect of PVCap-XA1 on the formation of methane hydrate

3.2.1. Constant temperature and constant volume method

Induction time was recorded for the inhibitor solution in an isothermal, constant-volume system. Figure 5 illustrates the hydrate formation process in pure water with the addition of 2.0 wt.% PVCap-XA1. The PVCap-XA1 system exhibits a pronounced delay in hydrate nucleation compared to the blank test, confirming its strong kinetic-inhibitory performance. Upon initiating stirring, the system containing 2.0 wt.% PVCap-XA1 shows an immediate slight pressure drop of approximately 0.1 MPa, accompanied by a minor temperature rise, likely due to the dissolution of methane gas into the aqueous phase. For approximately 240 min, both temperature and pressure remain nearly constant, followed by a sudden pressure drop and a concurrent temperature increase, indicating rapid methane hydrate formation. This exothermic process results from the absorption of methane by the water phase to form clathrate hydrates. In contrast, the induction time in the methane–water system without inhibitor is nearly zero, as hydrate formation begins immediately upon stirring. These observations demonstrate the efficiency of 2.0 wt.% PVCap-XA1 in delaying the onset of methane hydrate formation and confirm its effectiveness as a potent kinetic inhibitor.

The inhibition efficiency was quantified as the induction-time delay relative to the blank system (Eq. 1). The calculated efficiencies increased with inhibitor concentration, reaching 94% for PVCap-XA1 and 62% for PVCap at 2.0 wt.%. These results confirm that the modified polymer provides a more substantial kinetic barrier to hydrate nucleation. As shown in Table 2, PVCap-XA1 consistently requires longer induction times to initiate hydrate formation, reflecting its enhanced surface adsorption and interfacial inhibition properties.

$$\eta(\%) = \frac{t_{inh} - t_{blank}}{t_{blank}} \times 100$$

where t_{inh} is the induction time in the presence of the inhibitor and t_{blank} is that of pure water.

3.2.2. Maximum subcooling

Maximum subcooling is defined as the extent to which an inhibitor-containing solution can be cooled below the hydrate equilibrium temperature before the onset of hydrate formation. It is determined under an isochoric, constant-rate cooling process. Operationally, subcooling is quantified as the temperature difference between the equilibrium hydrate temperature at the observed pressure and the onset temperature (T_o) at which hydrate formation is first detected [25]. Higher values of maximum subcooling indicate stronger inhibition, reflecting a more pronounced downward shift of the hydrate formation temperature from its equilibrium value.

Figure 6 presents a typical hydrate formation curve for a system containing 2.0 wt.% PVCap-XA1 inhibitor, measured using the constant-cooling method. The curve shows a considerably lower on-

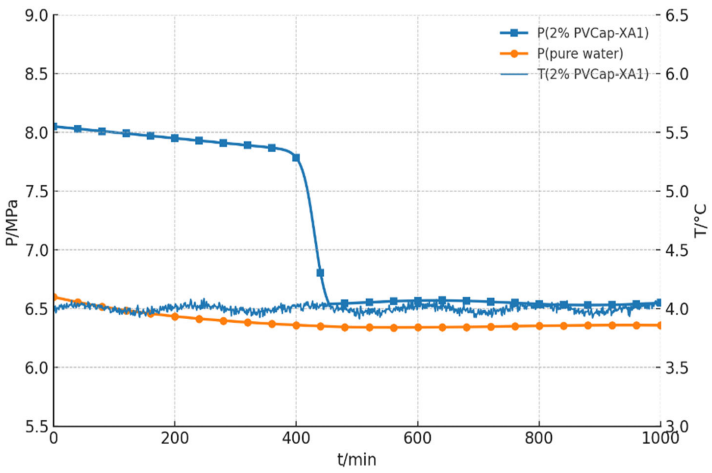

Fig. 5. Pressure–temperature behavior during methane-hydrate formation with and without 2.0 wt % PVCap-XA1.

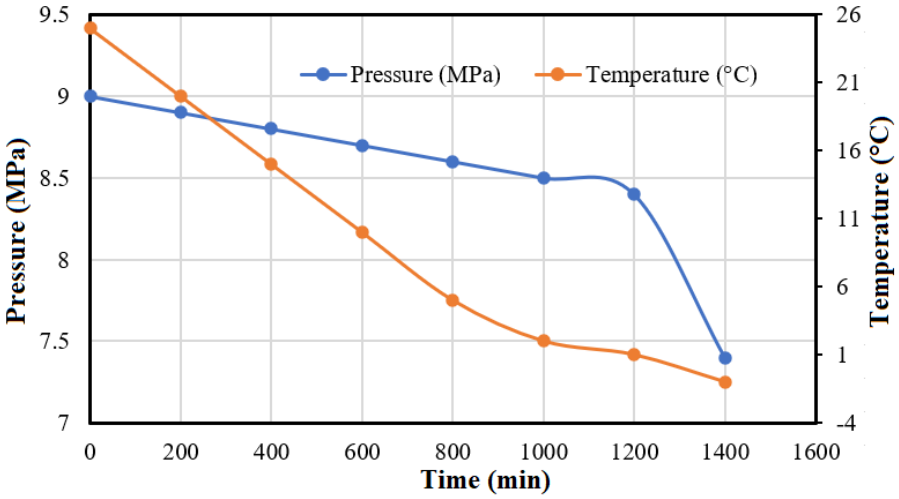

Fig. 6. Constant-cooling hydrate-formation path for 2.0 wt.% PVCap-XA1.

set temperature and a larger subcooling margin, reflecting enhanced resistance to hydrate formation under identical cooling conditions. Upon the start of stirring, both pressure and temperature in the reaction vessel decrease linearly at a constant rate. After approximately 1460 min, a steep pressure drop indicates the onset of hydrate formation. A moderate temperature increase is observed due to the initially small hydrate fraction and the rapid dissipation of heat released during crystallization. Hydrate formation is identified at the inflection point of the pressure–time curve, where the sharp pressure drop occurs; the onset pressure and temperature are recorded at this point. Maximum subcooling is defined as the difference between the equilibrium hydrate temperature at the onset pressure and the observed onset temperature. For the system with 2.0 wt.% PVCap-XA1, the onset occurred at 0.9 °C, and the maximum subcooling reached up to 10.5 °C, indicating that PVCap-XA1 offers strong resistance to hydrate formation.

The crystallization temperature of hydrate (T_0) and maximum subcooling degree for systems containing 0.5%, 1.0%, and 2.0% (mass) PVCap and PVCap-XA1 are listed in Table 1. All values reported in Table 1 are the mean ± standard deviation (n = 3) of independent experiments performed under the same operating conditions. The low deviations (<3.5%) reflect the excellent reproducibility of the hydrate-inhibition tests and confirm the precision of the measurements. Pure water serves as the blank control group, without the addition of any kinetic inhibitor. For the inhibitor-free system (pure water), the hydrate onset occurs at 8.8 °C, with a corresponding subcooling of 3.0 °C. These values are consistent with previously reported results in the literature [18, 26]. More importantly, with the addition of the inhibitor PVCap or PVCap-XA1, even at different mass fractions, the degree of subcooling in the system is significantly greater than that of the pure water sample. This result demonstrates the efficiency of these inhibitors in delaying hydrate formation by increasing the subcooling threshold. The system with 2.0% (mass) PVCap-XA1 exhibits the greatest subcooling of 10.5 °C. This indicates a gain of 7.5 °C relative to the pure methane hydrate system, indicating that PVCap and PVCap-XA1 strongly inhibit methane hydrate formation.

Figure 7 shows the maximum subcooling degree for PVCap-XA1 and PVCap at different concentrations. Data are presented as mean ± SD (n = 3). Both polymers exhibit increased subcooling with concentration, but PVCap-XA1 consistently demonstrates higher inhibition efficiency, reflecting enhanced interfacial activity due to its dual-functional modification. As the concentration increases from 1.0 wt.% to 2.0 wt.%, the maximum subcooling degree rises by 1.4 °C for PVCap-XA1 and by 2.2 °C for PVCap. At 1.0 wt.%, the subcooling of PVCap-XA1 is 3.4 °C higher than that of PVCap. These results indicate that PVCap-XA1 exhibits significantly improved inhibitory performance, particularly at lower concentrations, demonstrating its effectiveness in mitigating methane hydrate formation.

The data in Table 1 represent the experimental values closest to the average across three repeated runs. PVCap-XA1 was used as a representative modified inhibitor to analyze data variability. Figure 8 shows the maximum subcooling values and the average deviation for repeated experiments, with data presented as mean ± SD (n = 3). Small deviation bars indicate excellent repeatability and stability of the

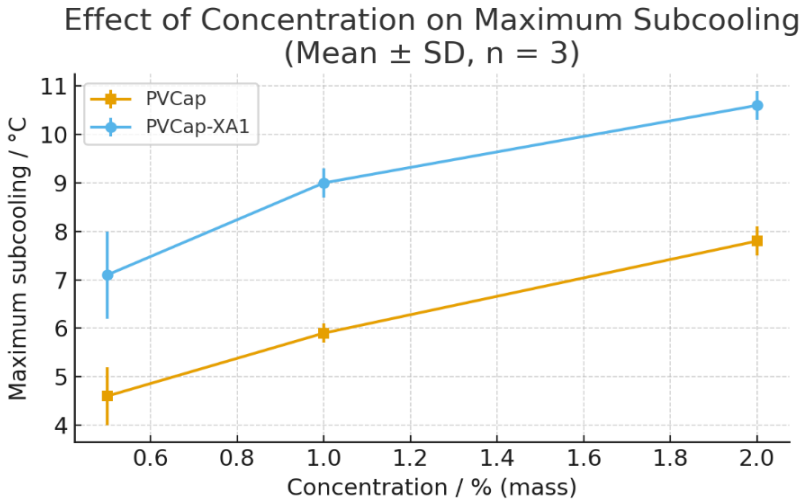

Fig. 7. Influence of inhibitor concentration on maximum subcooling.

Table 1. T_0 the maximum subcooling of PVCap and PVCap-XA1 at different concentrations

Sample	Concentration (% mass)	Induction time (min)	Crystallization temperature (°C)	Maximum subcooling temperature (°C)
Pure water	–	15 ± 1.0	9.06±0.3	3.09±0.3
PVCap	0.5	62 ± 3.0	7.42±0.4	4.64±0.2
PVCap	1.0	118 ± 4.0	5.46±0.3	5.87±0.2
PVCap	2.0	220 ± 5.0	3.50±0.3	8.14±0.3
PVCap–XA1	0.5	120 ± 4.0	4.43±0.2	7.21±0.3
PVCap–XA1	1.0	180 ± 5.0	2.58±0.2	9.37±0.3
PVCap–XA1 PVCap–XA1	2.0	255 ± 6.0	0.93±0.1	10.82±0.2

experimental results. Each run (1–3) shows an independent experiment conducted under the same conditions. The bold yellow line indicates the average ± standard deviation (n = 3), demonstrating excellent reproducibility with minimal differences between runs. As shown in Fig. 8, the measured values in Table 1 are very close to the averages. In terms of absolute error, the maximum occurs at 0.5 wt.%, which is 0.9 °C away from the average value. At this time, the relative error is 12.9%. Relative errors for the other data points were within 3.5%, confirming the high reproducibility of the measurements.

Experimental reproducibility was ensured by performing triplicate runs for each induction time and subcooling measurement. The values reported in Table 1 and Figs. 5–8 were obtained from the average of triplicate runs, with error bars used to show standard deviations. Only at 0.5 wt.% was the highest relative deviation of 12.9% observed; all other data points had deviations within ±3.5%, indicating excellent repeatability in inhibition performance.

3.3. Effect of PVCap-XA1 on the crystal morphology of methane hydrate

X-ray powder diffraction (XRD) of powdered crystalline materials can be used effectively to determine the crystallography of methane hydrates. Figure 9 shows PXRD patterns for methane hydrate formation with and without a 2.0 wt.% additive of PVCap-XA1 inhibitor; this illustrates that the methane hydrate formed is a type I hydrate [26]. All the samples have the sI hydrate structure, but in the PVCap-XA1 pattern, the peak-intensity ratio of (321)/(320) is reduced, demonstrating suppression of anisotropic growth and smaller crystallite dimensions. The characteristic peaks at 2θ = 27.3°, 28.4°, 30.4°, 31.4°, and 32.3° correspond to the respective crystal planes of (320), (321), (400), (410), and (411) crystal planes, respectively [27]. The star (*) marked peak in Fig. 9 indicates the presence of ice, while the numerically marked peaks correspond to methane hydrate [28].

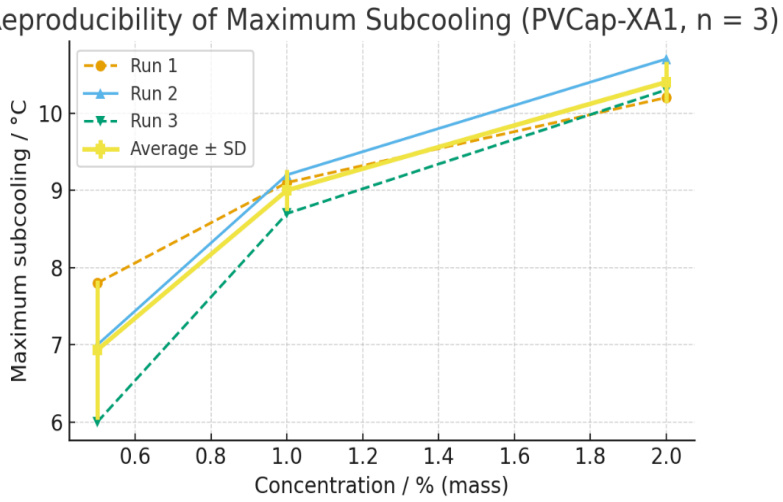

Fig. 8. Reproducibility of maximum-subcooling measurements for PVCap-XA1.

Comparison of the PXRD patterns for hydrates formed in neat water and with the addition of 2.0 wt.% PVCap-XA1 shows no change in the crystallographic structure of methane hydrate: peak positions (and their indices) are the same as those for the neat hydrate within experimental resolution. PVCap-XA1 thus primarily acts as a kinetic inhibitor, suppressing nucleation and growth without altering the underlying lattice topology.

X-ray diffraction peak intensities depend on the type of atom, the number of atoms, and their positions in the unit cell. Based on this, the peak intensity in a pure water system is higher; hence, the hydrate purity in the pure water sample is also higher. Since it was impossible to control all factors affecting sample-specific variations, relative peak intensities within the same sample were compared to ensure consistency in the analysis. The intensity ratio of the diffraction peaks of the crystal planes (321) and (320) is 2.6 in the pure water-methane system, while this ratio decreases to 2.15 in the system containing 2.0% (mass) PVCap-XA1. The decrease in the (321)/(320) peak-intensity ratio indicates preferential adsorption of PVCap-XA1 on specific planes, which alters the relative diffracted intensities and leads to anisotropic growth kinetics in methane hydrate.

Raman spectroscopy clearly reveals the distribution of guest molecules within hydrate cages. As shown in Fig. 10, methane hydrates formed in pure water and PVCap-XA1–containing media both exhibit a prominent band near 2905 cm^{-1} (CH_4 in large $5^{12}6^2$ cages) and a weaker one near 2915 cm^{-1} (CH_4 in small 5^{12} cages). In a related manner, increased inhibition efficiency and decreased cage occupancy of methane with rising inhibitor loading are mirrored by a progressive decrease in the IL/IS (large-to-small cage) ratio. Their local positions and relative intensities, which vary with PVCap-XA1 concentration, provide insights into cage occupancy and regional structure, enabling direct assessment of structural properties under formation conditions.

PXRD patterns of pure methane hydrate and PVCap-XA1-treated samples were evaluated for any quantifiable changes in crystallographic orientation. The I_{321}/I_{320} intensity ratio between the (321) and (320) diffraction peaks decreased from 2.60 ± 0.05 in the pure hydrate to 2.15 ± 0.04 in the PVCap-XA1 sample. The reported values show the mean ± SD of three independent measurements. A Student's t-test ($\alpha = 0.05$) confirmed that this reduction is statistically significant ($p < 0.05$), hence, that PVCap-XA1 elicits a measurable change in lattice orientation and preferred growth direction during hydrate formation. The reduced ratio suggests inhibition of growth of the (321) plane, leading to smaller, more isotropic crystallites, as observed by SEM.

The v_1 symmetric stretching band of the 5^{12} (small-cage) framework [29, 30] was analyzed by comparing Raman peak positions of hydrates formed in PVCap-XA1 solutions at different concentrations with those formed in neat water. There was no significant difference, which suggests that PVCap-XA1 does not alter the crystal structure of methane hydrate. This observation is consistent with the conclusions from the earlier PXRD analysis. It can be considered the ratio of large cages to small cages. The measure is the large-to-small-cage ratio, defined by the $5^{12}6^2$ to 5^{12} Raman intensity ratio IL/IS. The theoretical ratio is 3.02 [31, 32]. In the methane water reference, the measured value is 2.97, which is close to the theoret-

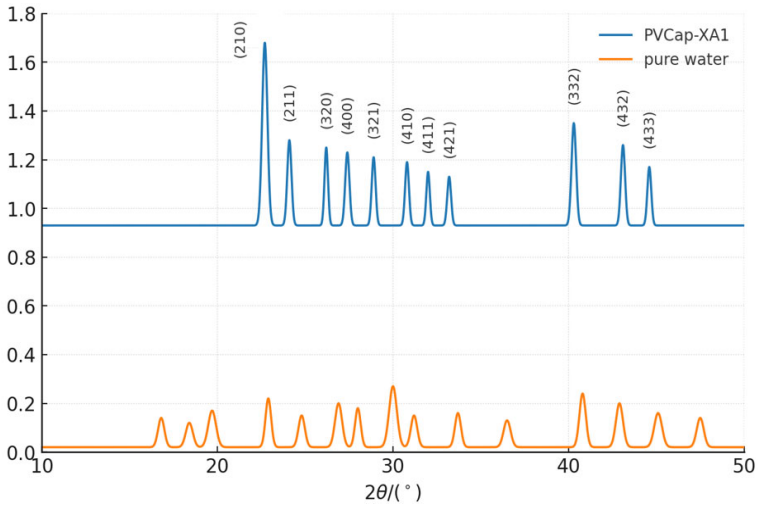

Fig. 9. PXRD patterns of methane hydrates formed in pure water, with PVCap, and with PVCap-XA1.

ical value, indicating that the measurements are valid. For PVCap-XA1 solutions at 0.5, 1.0, and 2.0 wt.%, the ratios decreased to 2.88, 2.71, and 2.54, respectively, all lower than the neat-water baseline. These results suggest that free methane molecules preferentially occupy the small cages during hydrate formation. This is in agreement with literature reports [32, 33], which attribute this preferential occupation to methane's significantly higher binding energy within small cages (E_b = –8.10 kcal/mol; 1 cal = 4.18 J) compared with large cages (E_b = –5.28 kcal/mol). The higher the binding energy, the more thermodynamically favorable it is for methane to occupy the small cages. This analysis clarifies how PVCap-XA1 affects cage occupancy during methane hydrate formation. It demonstrates that the inhibitor alters guest distribution rather than the crystal lattice itself, supporting the proposed inhibitory mechanism.

PVCap-XA1 reduces the IL/IS ratio by restricting methane access to hydrate cages. The copolymer attaches to forming hydrate surfaces through hydrogen bonds, forming steric barriers that hinder methane diffusion through cage openings. As a result, CH_4 is selectively trapped in the smaller, more stable cages, leaving many larger cages empty, thereby lowering the IL/IS ratio and enhancing lattice stability. Kinetically, PVCap-XA1 prevents hydrate formation by disrupting even cage occupancy and maintaining fewer large cages. These results agree with earlier research on steric hindrance controlling hydrate kinetics [32].

The IL/IS ratio, which reflects the relative occupancy of large to small hydrate cages, decreased with increasing PVCap-XA1 concentration – from 2.97 (blank) to 2.54 (2.0 wt.%). This decrease correlates well with the increased induction time (from

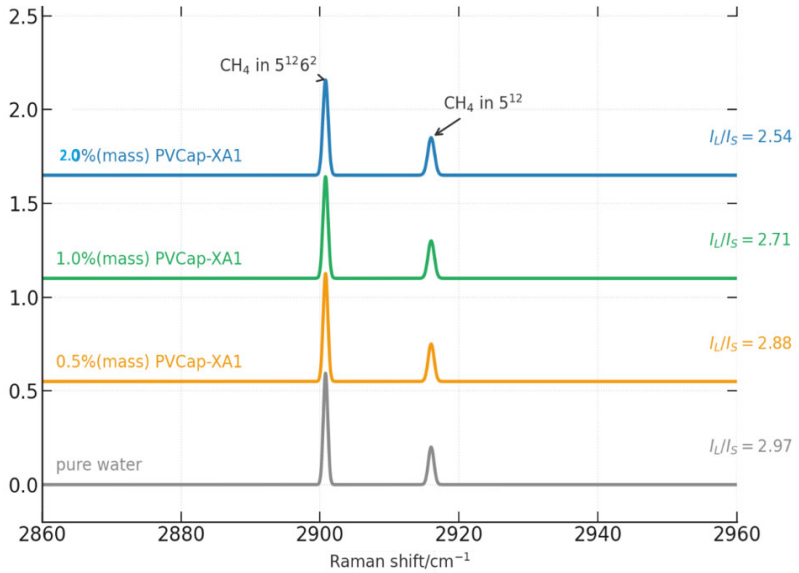

Fig. 10. Raman spectra of methane hydrates at different PVCap-XA1 concentrations.

15 to 240 min) and higher maximum subcooling, confirming that structural distortion, as directly detected in Raman spectra, corresponds to enhanced inhibition efficiency. A strong correlation (R^2 = 0.93) was obtained between IL/IS ratio and inhibition efficiency, showing that PVCap-XA1 acts not only to change cage occupancy but also to delay hydrate nucleation effectively. These results confirm that PVCap-XA1 not only alters hydrate cage occupancy but also effectively delays hydrate nucleation.

3.4. Influence of PVCap-XA1 on Methane Hydrate Morphology

The micromorphology of methane hydrate was examined using cryogenic scanning electron microscopy (cryo-SEM). Figure 11 shows the crystal morphologies of methane hydrates formed in pure water and in a system containing 2.0 wt.% PVCap-XA1. In pure water, the methane hydrate crystals exhibit a dense, highly regular pore structure, characteristic of submicron-scale porosity [33, 34]. This porous architecture facilitates methane diffusion into the crystals, thereby promoting the formation of additional hydrate cages.

In contrast, the addition of 2.0 wt.% PVCap-XA1 markedly alters the crystal morphology. Hydrate crystals in this system display a fish-scale-like structure, with particles accumulating in dense, layered formations. This layered morphology forms a thicker, less permeable surface, effectively hindering the diffusion of methane gas into the hydrate lattice. Consequently, PVCap-XA1 suppresses hydrate formation by physically obstructing the methane molecules from accessing the hydrate cages. The observed trend highlights PVCap-XA1's inhibition of methane hydrate formation by altering crystal morphology, thereby disrupting the required porosity for gas diffusion within the hydrate structure.

3.5. Mechanistic Insight into PVCap-XA1 Inhibition of Methane Hydrate Formation

The chemical backbones of PVCap-XA1 and PVCap (Fig. 1b–c) both contain highly hydrophilic amide groups. During and before nucleation, these amide groups hydrogen-bond with interfacial water, anchoring the polymers to form hydrate surfaces [35]. Continuous surface adsorption blocks crystal growth by creating steric obstacles at cage entrances, thus preventing CH_4 entry and inhibiting methane hydrate nucleation and growth [36].

PVCap-XA1 inhibits more effectively than PVCap because its backbone also contains hydrophobic ester and alkoxy groups. Consistent with previous findings that hydrophobic blocks improve kinetic hydrate inhibitors [37]. These groups disrupt the local hydrogen-bond network of water, increase structural distortions, and further slowdown cage growth and formation [38]. Zou et al. [39] demonstrated that hydrophobic alkoxy functionalities improve inhibitor chain conformation, increase surface area, and strengthen interfacial interactions with hydrate cages. In PVCap-XA1, the amide groups anchor to the hydrate surface, while the hydrophobic ester and alkoxy segments reorganize nearby water molecules, disrupting the well-coordinated hydration network required for cage formation. This amphiphilic action effectively prevents nucleation and subsequent crystal growth.

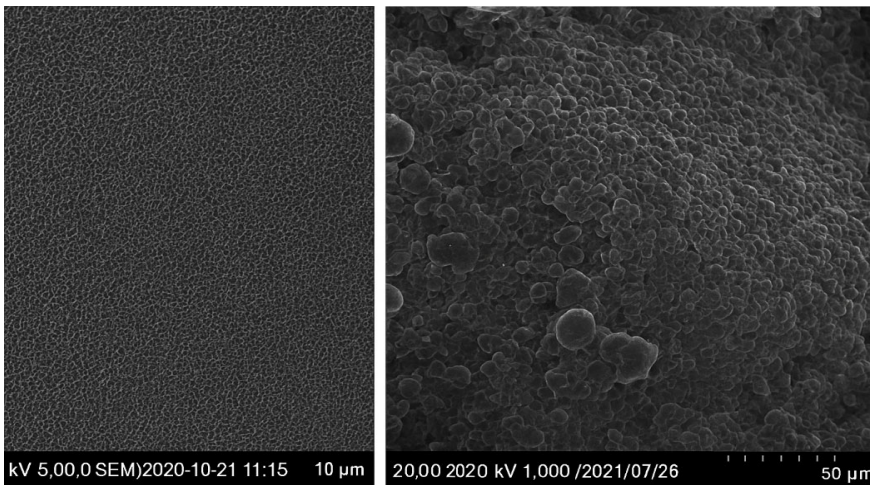

Fig. 11. Microstructural images of methane hydrate crystals formed in the presence of 2.0 wt.% PVCap-XA1 compared to those formed in pure water.

4. Conclusion

In this work, a novel kinetic hydrate inhibitor, PVCap-XA1, was synthesized. Its molecular structure is similar to that of the existing inhibitor PVCap, with a modified terminal chain containing oxyethylene and ester groups. The inhibitory performance, crystal structure, and micromorphology of methane hydrates formed in the presence of PVCap-XA1 were systematically investigated.

1. *Inhibitory performance.* Under identical conditions, adding 2.0 wt.% PVCap-XA1 extended the hydrate induction time to approximately 240 min compared to pure water and methane controls. This concentration also resulted in a significantly higher maximum subcooling than PVCap alone, indicating superior kinetic inhibition. Mechanistically, the hydrophobic ester and alkoxy groups along the PVCap-XA1 backbone disrupt the local hydrogen-bond network of water that is essential for hydrate cage formation, thereby suppressing nucleation and slowing subsequent hydrate growth.

2. *Crystal structure effects.* X-ray diffraction confirmed that methane hydrate retains its clathrate crystal structure in the presence of PVCap-XA1. The inhibitor induces a redistribution of relative diffraction intensities, particularly at the (321) and (320) reflections, suggesting facet-specific interactions with the growing crystal. Correspondingly, the CH_4 Raman I_L/I_S ratio ($5^{12}6^2$ large cages: 5^{12} small cages) decreases with the addition of PVCap-XA1, which aligns with inhibited methane incorporation into large cages. Overall, these results support a kinetic model in which PVCap-XA1 blocks large-cage occupation and, consequently, slows hydrate growth.

3. *Micromorphology analysis.* Cryogenic scanning electron microscopy disclosed dramatic changes in the morphology of hydrate crystals upon adding PVCap-XA1. Methane hydrates formed in pure water are porous and highly favorable for the diffusion of methane gas and hydrate formation. On the contrary, methane hydrates formed with PVCap-XA1 exhibited a characteristic "fish scale" morphology with a very dense, layered structure. This denser morphology most likely acts as a barrier, preventing methane gas from entering the hydrate cages and thereby further inhibiting hydrate formation.

These findings demonstrate that PVCap-XA1 inhibits methane hydrate formation through its unique molecular structure and selective interaction with hydrate crystal planes. Delayed nucleation, selective interaction with the crystal plane, and morphological changes in hydrates established PVCap-XA1 as a highly effective kinetic inhibitor for methane hydrate formation.

Although the present study clearly establishes that PVCap-XA1 exhibits superior kinetic inhibition of hydrate formation under the more controlled conditions of the laboratory, further work is needed to explore its performance under conditions closer to those of real operations. Additional research on PVCap-XA1 should focus on dynamic flow-loop systems and realistic gas-mixture compositions, with gas composition, flow turbulence, and pressure fluctuations closer to those in the field. These studies would yield much-needed information on the long-term stability, regeneration capability, and scalability of PVCap-XA1 for industrial hydrate mitigation applications.

Acknowledgments

The authors would like to thank Tikrit University and Universiti Malaysia Pahang for providing a laboratory.

References

[1]. J.D. Sundramoorthy, P. Hammonds, B. Lal, G. Phillips, Gas hydrate gas hydrate equilibrium measurement and observation of gas hydrate dissociation with/without a KHI, *Procedia Eng.* 148 (2016) 870–877. DOI: 10.1016/j.proeng.2016.06.476

[2]. J. Xu, M. Tang, T. Liu, L. Fan, Technological paradigm-based development strategy towards natural gas hydrate technology, *Energy* 289 (2024) 129956. DOI: 10.1016/j.energy.2023.129956

[3]. C. Tang, X. Zhou, D. Li, In situ Raman investigation on mixed CH_4-C_3H_8 hydrate dissociation in the presence of polyvinylpyrrolidone, *Fuel* 214 (2018) 505–511. DOI: 10.1016/j.fuel.2017.11.063

[4]. S. Yousefi, M. Bahrami, S. Hesam Najibi, Hydrate phase equilibria of carbon dioxide/propane gas mixture in concentrated aqueous sodium chloride solutions: Experimental data and prediction, *J. Mol. Liq.* 376 (2023) 121417. DOI: 10.1016/j.molliq.2023.121417

[5]. L. Wan, N. Zhang, D.-Q. Liang, Inhibition effects of polysaccharides for gas hydrate formation in methane–water system, *J. Mol. Liq.* 292 (2019) 111435. DOI: 10.1016/j.molliq.2019.111435

[6]. M. Aminnaji, B. Tohidi, R. Burgass, M. Atilhan, Gas hydrate blockage removal using chemical injection in vertical pipes, *J. Nat. Gas Sci. Eng.* 40 (2017) 17–23. DOI: 10.1016/j.jngse.2017.02.003

[7]. Q. Nasir, H. Suleman, Y.A. Elsheikh, A review on the role and impact of various additives as promoters/inhibitors for gas hydrate formation. *J. Nat. Gas Sci. Eng.* 76 (2020) 103211. DOI: 10.1016/j.jngse.2020.103211

[8]. M.R. Talaghat, Intensification of the performance of kinetic inhibitors in the presence of polyethylene oxide and polypropylene oxide for simple gas hydrate formation in a flow mini-loop apparatus, *Fluid Phase Equilib*. 289 (2010) 129–134. DOI: 10.1016/j.fluid.2009.11.025

[9]. A. Farhadian, A. Shadloo, X. Zhao, et al., Challenges and advantages of using environmentally friendly kinetic gas hydrate inhibitors for flow assurance application: A comprehensive review, *Fuel* 336 (2023) 127055. DOI: 10.1016/j.fuel.2022.127055

[10]. Y. Salamat, A. Moghadassi, M. Illbeigi, et al., Experimental study of hydrogen sulfide hydrate formation: Induction time in the presence and absence of kinetic inhibitor, *J. Energy Chem.* 22 (2013) 114–118. DOI: 10.1016/S2095-4956(13)60015-7

[11]. M. Aghajanloo, M. Reza Ehsani, Z. Taheri, Kinetics of methane+ hydrogen sulfide clathrate hydrate formation in the presence/absence of poly N-vinyl pyrrolidone (PVP) and L-tyrosine: Experimental study and modeling of the induction time, *Chem. Eng. Sci.* 250 (2022) 117384. DOI: 10.1016/j.ces.2021.117384

[12]. T. Saikia, V. Mahto, Experimental investigations of clathrate hydrate inhibition in water based drilling fluid using green inhibitor, *J. Pet. Sci. Eng.* 147 (2016) 647–653. DOI: 10.1016/j.petrol.2016.09.022

[13]. A. Bakhtyari, A. Rasoolzadeh, K. Mehrabi, 11 - Natural gas thermodynamic hydrate inhibitors, in Advances in Natural Gas: Formation, Processing, and Applications. Vol. 3: Natural Gas Hydrates. 2024, p. 233-277. DOI: 10.1016/B978-0-443-19219-7.00003-5

[14]. Q. Wu, N. Lin, L. Li, et al., Experimental Study on the Kinetics of the Natural Gas Hydration Process with a NiMnGa Micro-/Nanofluid in a Static Suspension System, *Water* 14 (2022) 745. DOI: 10.3390/w14050745

[15]. Y. Wang, S. Fan, X. Lang, Reviews of gas hydrate inhibitors in gas-dominant pipelines and application of kinetic hydrate inhibitors in China, *Chin. J. Chem. Eng.* 27 (2019) 2118–2132. DOI: 10.1016/j.cjche.2019.02.023

[16]. J. Kondori, S. Zendehboudi, M.E. Hossain, A review on simulation of methane production from gas hydrate reservoirs: Molecular dynamics prospective, *J. Pet. Sci. Eng.* 159 (2017) 754–772. DOI: 10.1016/j.petrol.2017.09.073

[17]. Z. Yin, Z.R. Chong, H.K. Tan, et al., Review of gas hydrate dissociation kinetic models for energy recovery, *J. Nat. Gas Sci. Eng.* 35 (2016) 1362–1387. DOI: 10.1016/j.jngse.2016.04.050

[18]. Q. Zhang, X. Shen, X. Zhou, D. Liang, Inhibition effect study of carboxyl-terminated polyvinyl caprolactam on methane hydrate formation, *Energy Fuels* 2017. 31 (2017) 839–846. DOI: 10.1021/acs.energyfuels.6b02603

[19]. L.H. Ree, M.A. Kelland, P.J. Roth, Rhiannon Batchelor, First investigation of modified poly (2-vinyl-4, 4-dimethylazlactone)s as kinetic hydrate inhibitors, *Chem. Eng. Sci.* 152 (2016) 248-254. DOI: 10.1016/j.ces.2016.06.031

[20]. S. Henderson, S. Mazloum, T. Gorlach, Methanol Partitioning Study Using an Innovative Hydrate Inhibitor Monitoring Technology. Conference paper: SPE International Conference on Oilfield Chemistry, 2017.

[21]. M.E. Rebolledo-Libreros, J. Reza, A. Trejo, D.J. Guzmán-Lucero, Evaluation of copolymers from 1-vinyl-3-alkylimidazolium bromide and N-vinylcaprolactam as inhibitors of clathrate hydrate formation, *J. Nat. Gas Sci. Eng.* 40 (2017) 114–125. DOI: 10.1016/j.jngse.2017.02.008

[22]. C. Tang, Y. Zhang, D. Liang, Investigation into the Inhibition of Methane Hydrate Formation in the Presence of Hydroxy-and Esteryl-Terminated Poly (N-vinylcaprolactam), *Energy Fuels* 36 (2022) 3848–3856. DOI: 10.1021/acs.energyfuels.1c04438

[23]. Z. Wei, Luyang Yu, Shuqing Lu, Yan Zhao, Reversibly Thermo-Responsive Materials Applied in Lithium Batteries, *Energy Storage Mater.* 61 (2023) 102901. DOI: 10.1016/j.ensm.2023.102901

[24]. B. Shaoqing, Q. Jing, N. Huali, Z. Limin, Preparation,electrospinning and characterization of p(NVCL-co-MAA), *New Chemical Materials* 4 (2013) 62–64.

[25]. H. Kakati, A. Mandal, S. Laik, Synergistic effect of Polyvinylpyrrolidone (PVP) and L-tyrosine on kinetic inhibition of CH_4+ C_2H_4+C_3H_8 hydrate formation, *J. Nat. Gas Sci. Eng.* 34 (2016) 1361–1368. DOI: 10.1016/j.jngse.2016.08.027

[26]. N. Wei, J. Pei, H. Li, et al., Classification of natural gas hydrate resources: Review, application and prospect, *Gas Sci. Eng.* 124 (2024) 205269. DOI: 10.1016/j.jgsce.2024.205269

[27]. A.M. Gambelli, F. Rossi, Experimental characterization of memory effect, anomalous self-preservation and ice-hydrate competition, during

methane-hydrates formation and dissociation in a lab-scale apparatus, *Sustainability* 14 (2022) 4807. DOI: 10.3390/su14084807

[28]. K. Kim, S.-G. Cho, J.-H. Sa, Natural hydrophilic amino acids as environment-friendly gas hydrate inhibitors for carbon capture and sequestration. *ACS Sustainable Chem. Eng*. 9 (2021) 17413–17419. DOI: 10.1021/acssuschemeng.1c07278

[29]. N. Daraboina, C. Malmos, N. von Solms, Synergistic kinetic inhibition of natural gas hydrate formation, *Fuel* 108 (2013) 749–757. DOI: 10.1016/j.fuel.2013.02.018

[30]. M.-C. Caumon, P, Robert, E. Laverret, et al., Determination of methane content in NaCl–H_2O fluid inclusions by Raman spectroscopy. Calibration and application to the external part of the Central Alps (Switzerland), *Chem. Geol.* 378 (2014) 52–61. DOI: 10.1016/j.chemgeo.2014.03.016

[31]. P. Naeiji, M. Pan, M. Luzi-Helbing, et al., Experimental and simulation study for the dissociation behavior of gas hydrates–part I: CH_4 hydrates, *Energy Fuels* 37 (2023) 4484–4496. DOI: 10.1021/acs.energyfuels.2c03984

[32]. Y. Wu, Y. He, T. Tang, M. Zhai, Molecular dynamic simulations of methane hydrate formation between solid surfaces: Implications for methane storage, *Energy* 262 (2023) 125511. DOI: 10.1016/j.energy.2022.125511

[33]. M. Pan, P. Naeiji, J.M. Schicks, Experimental and Simulation Study for the Dissociation Behavior of Gas Hydrates–Part II: sII Mixed Gas Hydrates. *Energy Fuels* 37 (2023) 4497–4514. DOI: 10.1021/acs.energyfuels.2c03985

[34]. Y. Xie, T. Zheng, J-R. Zhong, et al., Experimental research on self-preservation effect of methane hydrate in porous sediments, *Appl. Energy* 268 (2020) 115008. DOI: 10.1016/j.apenergy.2020.11500

[35]. V.W.S. Lim, P.J. Metaxas, M.L. Johns, et al., The delay of gas hydrate formation by kinetic inhibitors, *Chem. Eng. J.* 411 (2021) 128478. DOI: 10.1016/j.cej.2021.128478

[36]. Kashish, M. Yusuf, M. Beg, et al., Natural gas hydrates: A review of various inhibitors and respective mechanisms, *J. Mol. Liq.* 403 (2024) 124809. DOI: 10.1016/j.molliq.2024.124809

[37]. M.S. Kamal, I.A. Hussein, A.S. Sultan, et al., Application of various water soluble polymers in gas hydrate inhibition, *Renew. Sustain. Energy Rev.* 60 (2016) 206–225. DOI: 10.1016/j.rser.2016.01.092

[38]. G. Wu, F. Coulon, J.-C. Feng, et al., Machine learning models for fast selection of amino acids as green thermodynamic inhibitors for natural gas hydrate, *J. Mol. Liq.* 370 (2023) 120952. DOI: 10.1016/j.molliq.2022.120952

[39]. X. Zou, M. Zi, K. Liu, et al., The molecular chain's length effect of alcohol and ether for synergistic enhancement with novel kinetic hydrate inhibitors in hydrate inhibition, *Fuel* 371 (2024) 131987. DOI: 10.1016/j.fuel.2024.131987